“Effect of Apex Cone Shape on Fine Particle Classification of Gas-cyclone”

Hideto Yoshida*, Yusuke Nishimura, Kunihiro Fukui and
Tetsuya Yamamoto

* Department of Chemical Engineering, Hiroshima University,
1-4-1, Kagamiyama Higashi-Hiroshima, 739-8527, Japan

Corresponding Author
Hideto Yoshida
Department of Chemical Engineering, Hiroshima University,
1-4-1, Kagamiyama Higashi-Hiroshima, 739-8527, Japan
Tel. +81+82-424-7853 FAX +81+82-424-5494
e-mail r736619@hiroshima-u.ac.jp

"Effect of Apex Cone Shape on Fine Particle Classification of Gas-cyclone"

Key Words: Gas-cyclone, Particle separation, Cut size, Particle size, Sub-micron particles

Abstract

The purpose of this paper is to study the effects of apex cone shape on particle separation performance of gas-cyclones by experiment and CFD studies. It is found that the optimum apex cone angle is 70 deg. The minimum 50% cut size was obtained by use of this special apex cone. From the flow visualization method by use of soap foam, the upward flow and downward flow coexisted on the surface of this special apex cone. The clear interface between upward flow and downward flow was detected on the apex cone angle of 70 deg. The effect of the apex cone angle on particle separation performance decreases under high inlet velocity conditions, because most particles are moving in the area away from the apex cone.

The particle separation performance and flow visualization results qualitatively supported the 3-dimensional CFD simulation based on the direct method.

Introduction

Gas-cyclones are widely used in separation or size classification apparatus for gas-solid flows because of their simple structure and low cost. Recently, with improvements in the dimensions of various parts of cyclones, a fairly high level of precision in the classification of sub-micron order particles has become possible［1-3］. Recent industrial requirements of ceramics or metal powders require particle size distributions with a narrow standard deviation, because the physical properties of such classified particles are related to the performance of electrical, magnetic and chemical reactions. In particular, particles with a diameter of 0.1 to 1 μm are required for various powder handling processes. In order to classify a particle cut size in the size range of 0.1 to 1μm, forced centrifugal classifiers are not always effective because of particle erosion problems and the increased maintenance costs of such classifiers due to high revolutions.

While Iinoya *et al.*［4］found that it is possible to classify powders even in the 0.4μm size range using special cyclones, it is generally difficult to change the cut size in a conventional cyclone separator. To solve this problem, Yoshida *et al.*［1, 5］ found that it is possible to change the cut size by the use of a moving circular guide plate at the cyclone inlet or by the use of an additional secondary flow injection method in the upper cylindrical part of the cyclone. By use of a special apex cone at the inlet part of the dust box and by using the blow-up method, it is reported that the cut size can be easily controlled from 1μm to 40μm size range［6］. In order to increase particle separation performance of a gas-cyclone, the effect of an apex cone used at the upper part of a dust box was examined and it is confirmed that rotational and upward fluid velocity components decreased with the apex cone set at the dust box［7］. However, the optimum shape of the apex cone in the gas-cyclone was not clear.

The purpose of this paper is to find the optimum apex cone shape in a gas-cyclone by use of simulation and experimental method. By use of the flow visualization method near the apex

cone, the optimum apex cone angle was determined. Interesting and new conclusions that can be used to increase particle separation performance of gas-cyclones are obtained.

1 Experimental apparatus

Figure 1 shows a schematic diagram of the gas-cyclone used in this study. The cyclone diameter was set at 72mm and each dimension was determined from experimental data that proved superior in classification performance［4］. The secondary flow injection method in the upper part of the cyclone as shown in Fig. 1 was used to improve classification performance ［5］. The performance of the cyclones were examined by use of the partial separation efficiency $\Delta\eta$ defined by:

$$\Delta\eta = \frac{m_c f_c \Delta D_p}{m_c f_c \Delta D_p + m_s f_s \Delta D_p} \qquad (1)$$

In the above equation, m_c and m_s are the masses of the collected particles in the coarse and fine sides, respectively. The particle size frequency distributions for each size range are indicated by f_c and f_s. Particle size distributions were measured by Laser-light scattering (Horiba Co., Ltd. LA-920). The experimental error in the partial separation efficiency was about 3 percent. A ring nozzle-type particle disperser (Nisshin Eng. Co., Ltd.) was installed after the screw feeder. The test particle used was Kanto Loam (JIS, Z8901, No. 11). The mass median diameter was 1.8μm and true density was 2900 kg/m^3. The total flow rate, including secondary flow rate of 100 l/min. was changed from 500 to 700 l/min. and powder flow rate was set about 2.0 g/min.

Figure 2 shows the dimensions of the test cyclone. In this study, various types of apex cones were used at the inlet part of the dust box. The cone angles examined were from 40 deg. to 80 deg. In general, the cone angle of 60 deg. is used in the gas-cyclone, but the optimum cone angle of the apex cone has not been clearly investigated. For each experiment, the spacing

between the bottom of the cylindrical part and the bottom of the apex cone was set to be 31.2 mm. Under this condition, the top position of the apex cone and the bottom of the cylindrical wall were set at nearly the same height.

2 Experimental results

Figure 3 shows the experimental results of the classification performance with and withoutthe apex cone. In this case, the cone angle of 60 deg. was used in the experiment. It is found that the 50% cut size with the apex cone in use was smaller than that without the apex cone. The decrease of particle collection efficiency without the apex cone might be particle re-entrainment from the dust box due to strong upward and rotational fluid components remained in the upper part of the dust box. To examine the flow differences with and without the apex cones, acryl particles of about 2 mm were initially set on the bottom of a transparent dust box. From the flow observations shown in Fig. 3, the acryl particles are lifted and moved to various directions in the case without the apex cone, but the moving particles are not detected in the case with the apex cone. This fact indicates that the upward and rotating fluid components remained in the dust box in the case without the apex cone and the probability of the outgoing particles from the dust box is increased. In order to clear the flow difference in the dust box, the flow visualization using water supplied on the bottom of the transparent dust box was carried out.

Figure 4 shows the experimental results of flow visualization with and without the apex cone. In case without the apex cone, violent changes in the liquid level was observed, but movement of the water surface is not detected in the case with the apex cone of 70 deg. The small change of water surface is detected with the apex cone of 40 deg. Then from the photographs shown in Fig. 4, high particle collection efficiency might be expected in the case with the apex cone of 70 deg.

The effect of apex cone angle on particle separation performance was examined and the experimental results are shown in Fig. 5. Figure 5-a and 5-b show the experimental results of particle separation performance for the main flow inlet velocity of 11 and 16.3 m/s, respectively. From the data of Fig. 5-a, the 50% cut size decreases as the apex cone angle increases. For the three cases, the minimum value of the 50% cut size was obtained for the apex cone angle of 70 deg. On the other hand, the 50% cut size is nearly equal under the high inlet velocity conditions as shown in Fig. 5-b. In this case, the apex cone angle of 70 deg. is better than the other cases, but the difference between each case is small. In order to find out the reasons why the experimental data shown in Fig. 5 was obtained, the numerical simulation and flow visualization method using soap foam around the apex cone region were carried out.

3 Numerical Simulation

In order to compare particle separation performance of various apex cone angles, the CFD simulation would be effective to find out the difference of physical phenomena around the apex cone region. The three-dimensional Navier-Stokes equations and equations of particle motions were solved numerically. Table 1 summarizes the basic equations used in the simulation. The direct flow method, that solves Navier-Stokes Equations directly, was used to calculate the flow field in the cyclone [8]. To calculate the non-linear convection terms, the artificial viscosity coefficient of 1/3 was selected to obtain a stable flow field [9]. The control volume method was used in the simulation [10].

Figure 6 shows the grid distributions for the various apex cone angles. In order to make clear the grid near wall region, the scales in horizontal and vertical directions are not the same. In order to calculate the partial separation efficiency for small particles, the radial grid spacing near the cylindrical, conical and the apex cone walls are designed to be as small as possible. The fluid boundary conditions on the wall, including the apex cone in the dust box, were set to

zero. Grid numbers in axial, radial and circumferential directions are 51, 44, and 53, respectively. The boundary-fitted curvilinear coordinate system was used in the simulation. In order to obtain reliable results in calculating small particle diameters, the radial grid spacing near the conical and cylindrical walls should be as small as possible. In the calculations, the equations of mono-sized particle motions were solved by the RKG method ［11］.

It was assumed that particles are collected when they touch the wall surface and particle repulsion was not taken into consideration. The particle trajectories of mono-sized particles are calculated, then calculated result does not depend on feed particle size distribution. In the experiment, inlet dust concentration was very small, so the interaction between particles and fluid was ignored in the simulation. Details of the calculation method are reported in our previous paper ［12］.

4 Flow around the apex cone

Figure 7 shows the fluid velocity vectors around the apex cone of the cone angle from 40 to 80 deg. For the apex cone angle of 40 deg., the upward velocity components are detected on the inclined surface of the apex cone. But for the apex cone angle of 70 deg., the critical line between upward flow and downward flow shown in the dotted line is detected and the downward flow velocity components are very small compared to the upward flow. The separation line between upward and downward flow is clearly found for the apex cone angle of 70 deg. The red circles in Fig.7 show the upward flow region. For the 70 deg. case, the upward flow region is observed in the upper half area, but the region is slightly increased for the 80 deg. case. Then it is considered that particles collected on the upper conical section might be easily moved to the central upward flow. In order to find out the critical line of the upward and downward flow on the inclined surface of the apex cone, visualization experiments were carried out by use of soap foam. Before running the experiments, all surfaces of the apex cone were

coated with white soap foam. Then inlet flow was introduced to the cyclone during 10 min., and the observation of the surface of the apex cone was carried out.

Figure 8 shows the enlarged photograph near the apex cone of 70 deg. The velocity vectors calculated by CFD simulations are also included in the photograph. For the lower part of the apex cone, a small amount of soap foam remained, but the soap foam is not detected on the upper zone of the apex cone. From the flow vectors, the upper and lower parts of the apex cone correspond to the upward and downward flow regions, respectively. The critical line of the soap foam might be considered to be the separation line of the upward and downward flows. Figure 9 shows the flow visualization photographs of soap foam with various kinds of apex cones. Also included in each photograph are the flow vectors calculated by CFD simulations. The area of soap foam remaining on the apex cone becomes maximum for the cone angle of 70 deg. The region without the soap foam corresponds to the upward flow and the region with soap foam corresponds to the downward flow. Then it is considered that upward fluid and particles of downward flow direction can be clearly separated with the apex cone at an angle of 70 deg. The particles collected on the upper region of the apex cone might be moved to the upward flow and not be collected. The probability of these escaping particles will be a minimum for the case of the apex angle of 70 deg. The fluid flow rates into the dust box for various apex cone angles are important. The maximum flow rate entering the dust box is obtained for the apex cone angle of 60 deg.

Figure 10 shows the relation between 50% cut size and apex cone angle. It is found that 50% cut size indicated the minimum value for the apex cone angle of 70 deg. The calculated results indicated by the dotted line also shows the minimum 50% cut size for the cone angle of 60～65 deg. These results of high collection efficiency for cone angle of 70 deg. agree with the photographs shown in Fig.9.

The particle trajectories calculated by CFD simulation are shown in Fig. 11. The initial starting positions of particles are set to the same points and three types of the apex cones are

used in each case. For the cone angle of 70 deg., the 1.3μm diameter particles are collected on the lower part of the apex cone. The particle collection place shown in Fig. 11-b corresponds to the down-flow region of the apex cone surface shown in Fig. 7-d. On the other hand, all particles are not collected for the apex cone angles of 40 and 80 deg. Due to the strong upward flow near these apex cone surface, the probability of particle collection will be decreased. For the apex cone angle of 40 deg., the particles entering into the lower part of the dust box move out of the dust box. The purpose of the apex cone set in the dust box is to decrease the fluid flow component, but the simulation results show that the apex cone angle of 40 deg. is ineffective.

Figure 12 shows the particle separation performance for the three kinds of apex cones. The minimum cut size is obtained for the apex cone angle of 70 deg. The 50% cut size decreases as the apex cone angle increases. The calculation results by use of CFD simulation is also shown and simulation results agree with the experimental results qualitatively. The difference between the experimental results and calculations might be the selection of the flow Reynolds number used in CFD simulation. To obtain the converged solution, the flow Reynolds number in CFD simulation selected was 3000. In the experiment, the flow Reynolds number was greater than 2 x 10^4 and the fluid viscosity effect might be overestimated in the CFD simulation. It is difficult to obtain the converged solution with flow Reynolds number greater than 3000. In Fig.12, the reason of difference between calculation and experiment might be flow Reynolds between them. When the solution of high Reynolds number calculation is obtained, the difference between experiment and calculation might be small. The results shown in Fig. 12, indicating high separation performance are obtained for the apex cone angle of 70 deg., agree with the data shown in Fig. 10.

5 Effect of apex cone angle under the high inlet flow condition

The previous section examines the particle separation performance under low inlet velocity condition. This section examines the separation performance under the condition of high inlet velocity.

Figure 13 shows the relation between 50% cut size and the apex cone angle under cyclone inlet velocity of 16.3 m/s. It is found that 50% cut size does not depend on the apex cone angle. The numerical results shown in the dotted line also indicated the same results. In order to find out the reason obtained in Fig. 13, the flow visualization experiments by use of soap foam under high inlet velocity condition was also carried out.

Figure 14 shows the experimental results taken from various apex cone angles. The general patterns are nearly equal to the data shown in Fig. 9. The area of soap foam is maximum for the cone angle of 70 deg. The region without the soap foam corresponds to the upward flow and the region with soap foam corresponds to the downward flow. Then it is considered that particles moving near this apex cone surface will be affected by the upward and downward flows.

Figure 15 shows the results of particle trajectories obtained by use of CFD simulation in the high inlet velocity condition. Figures 15-a and 15-b correspond to the particle diameter of 1.3 and 1.0μm, respectively. For the 1.3μm particles, the particles are collected on the cylindrical wall region and are not affected by the flow difference near the apex cone. On the other hand, for the 1.0μm particles, the particles move to the lower zone of the cylindrical wall due to the high inlet flow velocity. But all particles are moving in places away from certain distance of the apex cone. Then, from the trajectory calculation shown in Figs. 15-a and b, the particles are not strongly affected by the flow difference near the apex cone. Under high velocity condition, the particles tend to move near the conical and cylindrical wall section due to the strong centrifugal effect. Then particles entering into the dust box tend to move away from the apex cone. When particles move near the apex cone region, separation performance will be affected by changes in the apex cone angle, but from the CFD simulation under the high inlet velocity condition, particles move away from certain distance of the apex cone.

Figure 16 shows the particle separation performance for the three kinds of apex cones under the condition of high inlet velocity. The experimental results of the partial separation efficiency curves are nearly equal for the three cases. The calculated results of the large particle diameter region for the cone angle of 70 deg. is slightly better than other cases, but the separation efficiency difference is very small. Because particles are moving away from the apex cone under the conditions examined, then the effect of apex cone angle on particle separation performance is very small under the high inlet velocity condition.

For the practical application of the cyclone separator, the apex cone used at the dust box is effective to decrease the magnitude of the fluid velocity components in the dust box. From these research results, the apex cone angle of 70 deg. is recommended to increase particle collection efficiency.

Conclusion

Effect of apex cone angle on particle separation performance was examined by use of experimental and CFD studies and the following conclusions are obtained.

(1) The optimum apex cone angle was 70 deg. under the low inlet velocity condition. By use of this apex cone angle, the minimum value of 50% cut size was obtained.

(2) From the flow visualization method by the use of soap foam, the upward flow and downward flow coexisted on the surface of the cone angle of 70 deg. The clear separation line between upward and downward flows is observed by use of this special apex cone.

(3) The effect of apex cone angle on particle separation performance becomes small under the high inlet velocity condition. Because nearly all particles are moving in places away from the apex cone, then the particle separation performance is not affected by changes of the apex cone angle.

(4) The particle separation performance and flow visualization results qualitatively agreed with

the 3-dimentional CFD simulation based on direct method.

Nomenclature

C Cunningham's slip correction factor (-)

C_D drag coefficient of particle (-)

D_p particle diameter (μm)

D_{p50} 50% cut size of cyclone (μm)

D cyclone diameter (m)

D_1 bottom diameter of apex cone (m)

E total collection efficiency of the cyclone (-)

$f_c(D_p)$, $f_s(D_p)$ particle size distributions of coarse and fine sides, respectively (-/μm)

g gravity acceleration (m/s^2)

G inlet width ratio (-)

G_1 gravitational parameter (m/s^2)

H spacing between bottom of cylindrical part and apex cone bottom as shown in Fig.2 (m)

m_c, m_s mass of the collected particles for coarse and fine sides, respectively (kg)

p dimensionless pressure (-)

Q, Q_t, q cyclone inlet flow, total flow rate and secondary flow rate, respectively (l/min)

Re (=$Du_0 \rho / \mu$) flow Reynolds number (-)

Rep (=$D_p \rho \sqrt{(u_z - v_z)^2 + (u_r - v_r)^2 + (u_\vartheta - v_\vartheta)^2} / \mu$) particle Reynolds number (-)

S_ϕ general function of production term (-)

t time (s)

$\bar{t}$ dimensionless time (-)

$\bar{r}$, $\bar{z}$ dimensionless radial and axial coordinates (-)

u_z, u_r, u_θ axial, radial and tangential fluid velocities (m/s)

u, v, w dimensionless axial, radial and tangential fluid velocities (-)

u_0 inlet velocity of cyclone (m/s)

v_z, v_r, v_θ axial, radial and tangential particle velocities (m/s)

$\Delta\eta$ partial separation efficiency (-)

ϕ general function of conservation equation (-)

θ circumferential coordinate (-)

Γ diffusion coefficient (-)

ν (=1/Re) dimensionless viscosity (-)

μ fluid viscosity (Pa・s)

ρ , ρ_p fluid and particle density (kg/m^3)

τ particle relaxation time (s)

κ accuracy of classification (-)

α apex cone angle (deg.)

References

(1) H. Yoshida, T. Saeki, T. Fujioka, T. Ueda and T. Fuyuki, “Fine Particle Separation by Revised Type Air-cyclone Classifier”, Kagaku Kogaku Ronbunshu, 19, (1993), 476-482

(2) H. Yoshida, T. Fujioka, K. Hashimoto and K. Nagahashi, “Effect of Blow-down on Fluid Flow and Particle Movement in Cyclone Classifier”, Kagaku Kogaku Ronbunshu, 21, (1995), 594-602

(3) H. Yoshida, T. Yamamoto, K. Okanishi and K. Iinoya, “Elaborate Classification of Fly-ash Particles by Bench Scale Air Cyclone”, Kagaku Kogaku Ronbunshu, 23, (1997), 363-370

(4) K. Iinoya, T. Fuyuki, Y. Yamada, H. Hisakuni and E. Sue, “Dry Sub-micron Classification by a Small Blow-down Cyclone”, KONA, Powder and Particle, 11, (1993), 223-227

(5) H. Yoshida, K. Ono and K. Fukui, “The Effect of a New Method of Fluid Flow Control on Sub-micron Particle Classification in Gas-cyclones”, Powder Technology, 149, (2005), 139-147

(6) H. Yoshida, S. Akiyama, K. Fukui and S. Taniguchi, “Effect of Apex Cone Height on Particle Classification Performance of Cyclone Separator”, Advanced Powder Technology, 14,3 (2003), 263-278

(7) H. Yoshida, K. Fukui, S.Akiyama and S.Taniguchi, “The Effect of a New Method of Fluid Flow Control on Sub-micron Particle Classification in Gas-cyclones”, Powder Technology, 149, (2005), 139-14

(8) T. Kawamura and K. Kuwabara, “Computation of High-Reynolds Number Flow around a Circular Cylinder with Surface Roughness”, AIAA 22nd Aerospace Sciences Meeting, 84-0340, Nevada (1984), 1-11

(9) T. Kawamura, “Numerical Study of High Reynolds Number Flow Around a Circular Cylinder”, Ph. D. Thesis , Tokyo Univ., Japan (1980)

(10) Patankar, S.V., “Numerical Heat Transfer and Fluid Flow”, Hemisphere Pub., Washington, USA, (1980), 113-137

(11) R. Toei, “Practice of Chemical Engineering Programming”, The Society of Chemical Engineers, Japan Ed., (1976), 148-154

(12) H. Yoshida, T. Saeki, K. Hashimoto and T. Fuyuki, “Size Classification of Submicron Powder by Air Cyclone and Three-dimensional Analysis”, J. Chem. Eng., Japan , 24, (1991), 640-647

Figures and Tables Captions

Fig. 15-a Calculated particle trajectories for high inlet velocity condition (D_p=1.3 μ m, Q_t=700 l/min., q=100 l/min.)

Fig. 15-b Calculated particle trajectories for high inlet velocity condition (D_p=1.0 μ m, Q_t=700 l/min., q=100 l/min.)

Fig. 16 Effect of apex cone angle on partial separation efficiency in the case of Q_t=700 l/min.

Table 1 Equations of fluid and particle motion

$$\frac{\partial}{\partial \bar{t}}(\bar{r}\,\phi)+\frac{\partial}{\partial \bar{z}}(\bar{r}u\phi)+\frac{\partial}{\partial \bar{r}}(\bar{r}v\phi)+\frac{1}{\bar{r}}\frac{\partial}{\partial\theta}(\bar{r}w\phi)=$$

$$\frac{\partial}{\partial \bar{z}}(\bar{r}\Gamma\frac{\partial\phi}{\partial \bar{z}})+\frac{\partial}{\partial \bar{r}}(\bar{r}\Gamma\frac{\partial\phi}{\partial \bar{r}})+\frac{\partial}{\bar{r}\partial\theta}(\Gamma\frac{\partial\phi}{\partial\theta})+S_\phi$$

ϕ	Γ	S_ϕ
u	ν	$-\bar{r}\,(\frac{\partial p}{\partial \bar{z}})$
v	ν	$-\bar{r}\frac{\partial p}{\partial \bar{r}}+w^2-\frac{\nu v}{\bar{r}}-\nu\frac{2}{\bar{r}}\frac{\partial w}{\partial\theta}$
w	ν	$-\frac{\partial p}{\partial\theta}-vw-\frac{\nu w}{\bar{r}}+\nu\frac{2}{\bar{r}}\frac{\partial v}{\partial\theta}$

Particle's Eq. of Motion

$$(\frac{d^2r}{dt^2}-r(\frac{d\theta}{dt})^2)=-(\frac{C_DRe_p}{24})\frac{1}{\tau}(\frac{dv}{dt}-u_r)$$

$$(2\frac{d\theta}{dt}\frac{dr}{dt}+r\frac{d^2\theta}{dt^2})=-(\frac{C_DRe_p}{24})\frac{1}{\tau}(r\frac{d\theta}{dt}-u_\theta)$$

$$\frac{d^2z}{dt^2}=-(\frac{C_DRe_p}{24})\frac{1}{\tau}(\frac{dz}{dt}-u_z)+G$$

$$\tau=\frac{C\,\rho_p D_p^2}{18\,\mu}\qquad G=g$$

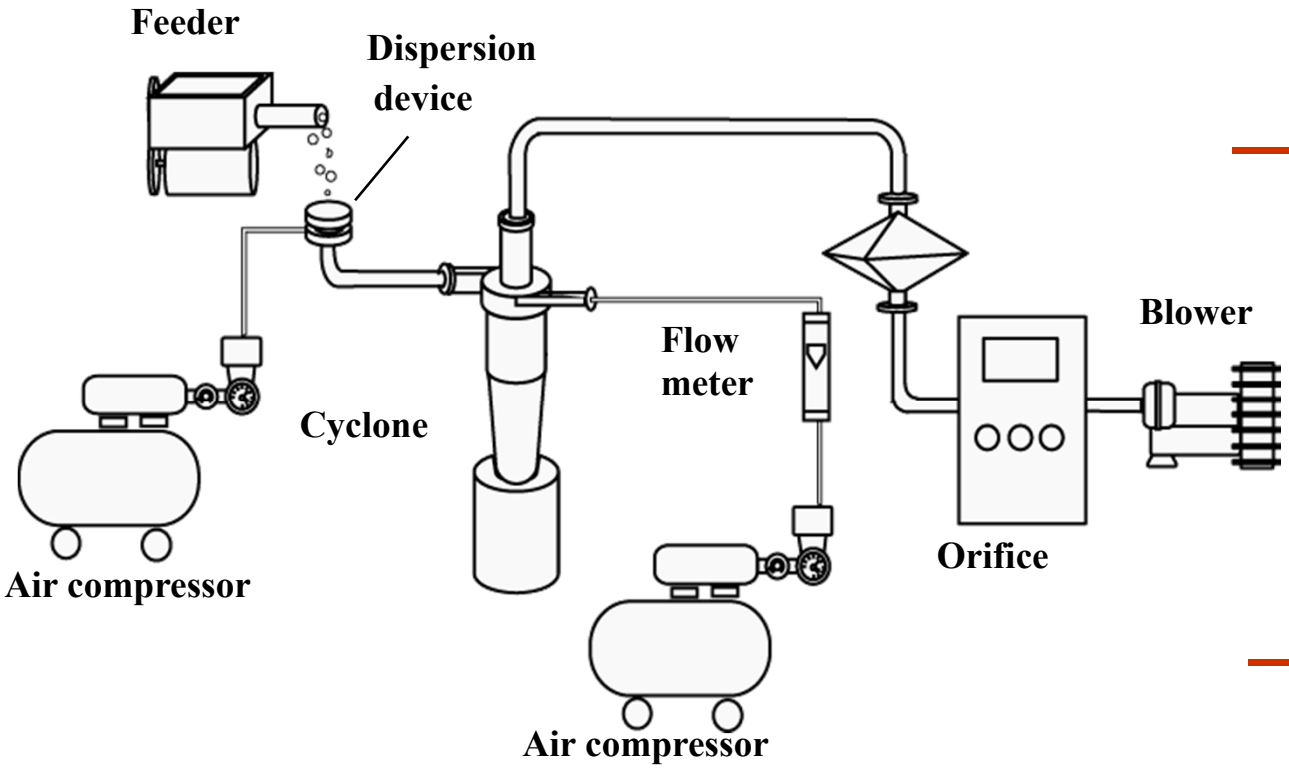

Experimental condition

Sample : Kanto Loam No. 11

Median diameter 1.8 μm

True density 2900 kg/m^3

Operating time : 10 min

Particle feed rate : 2.0 g/min

Secondary flow rate q : 100 L/min

Total flow rate, Q_t : 500-700 L/min

Cone height, H : 31.2 mm

Fig.1 Experimental apparatus

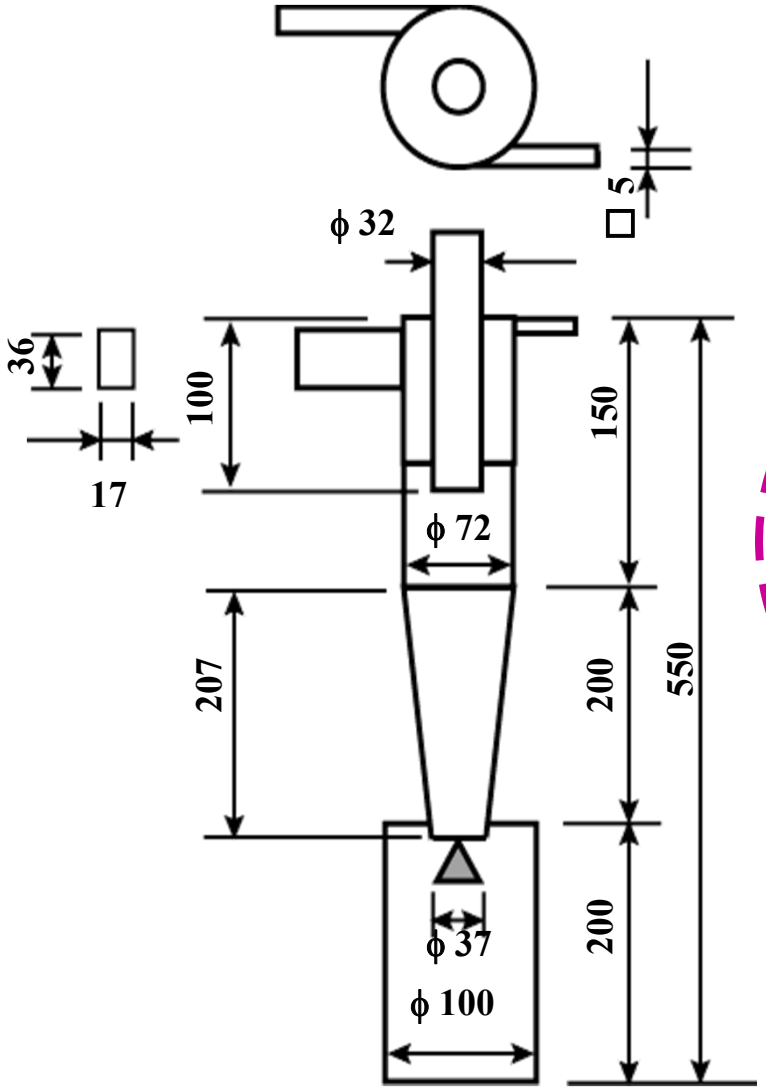

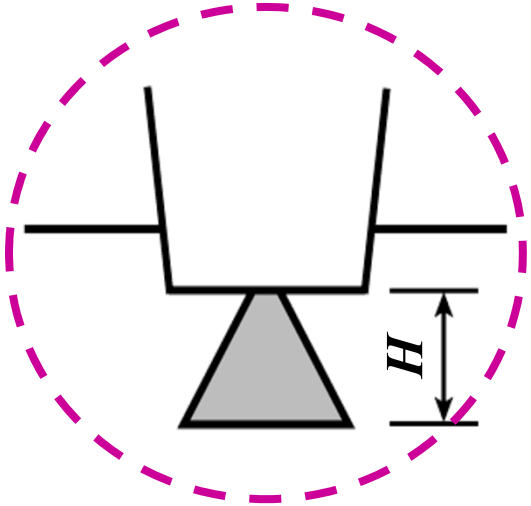

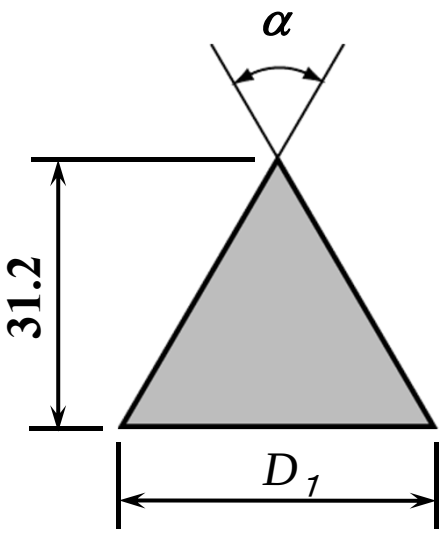

Type of cones

α [deg.]	40	50	60	70	80
D_1 [mm]	22.7	29.1	36.0	44.0	52.3

Fig.2 Dimension of cyclone

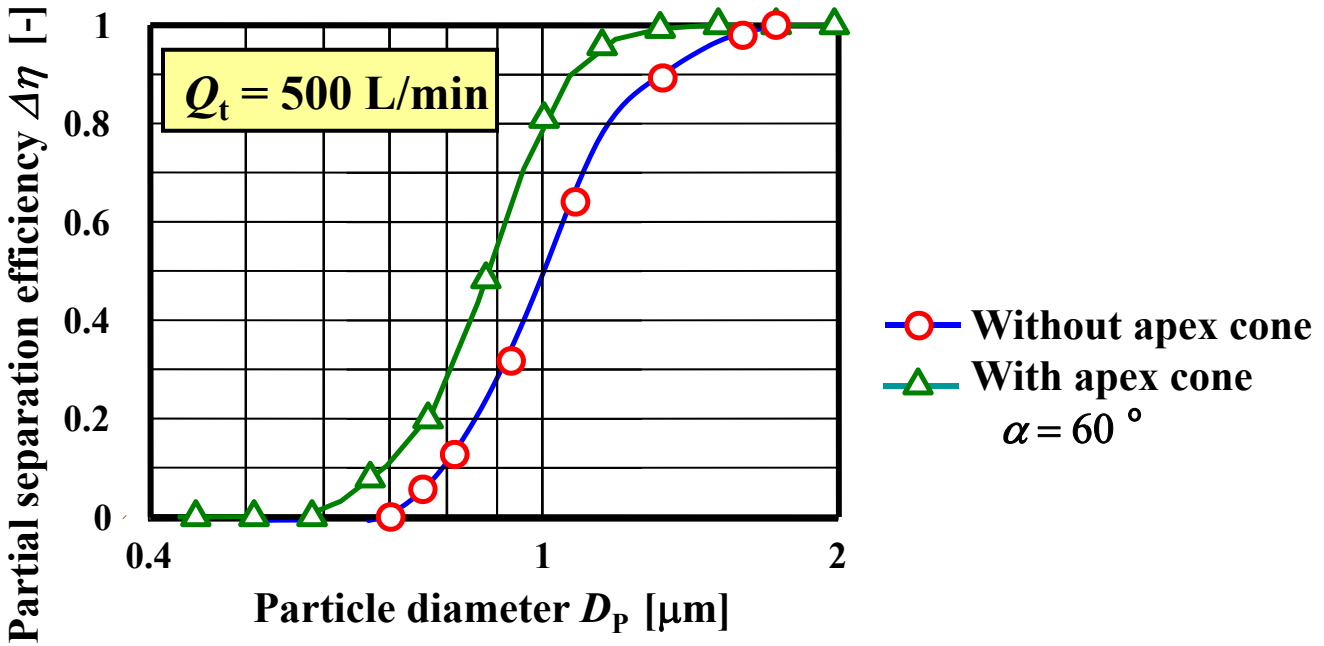

(a) Without cone

(b) With cone

Fig. 3 Separation performance and visualization of the dust box with and without apex cone (Q_t = 500 l/min)

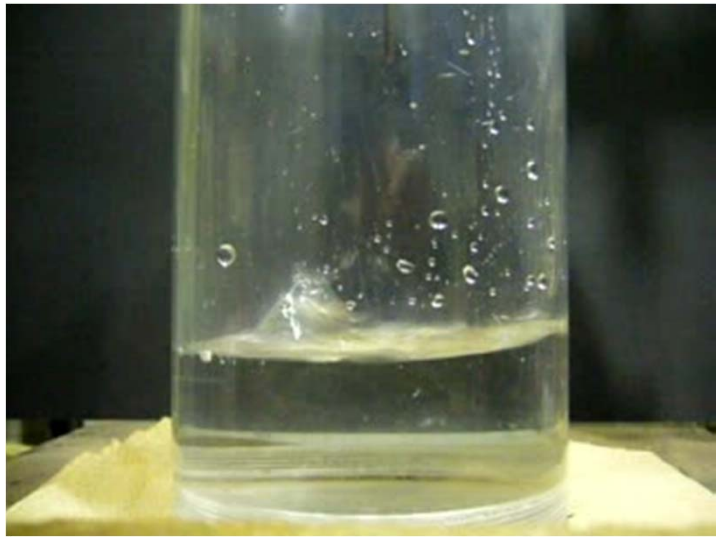

(a) Without cone

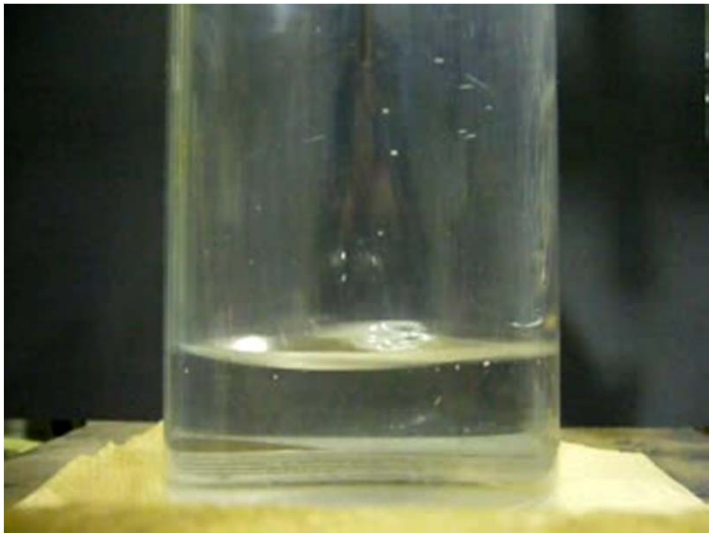

(b) $\alpha = 40^{o}$

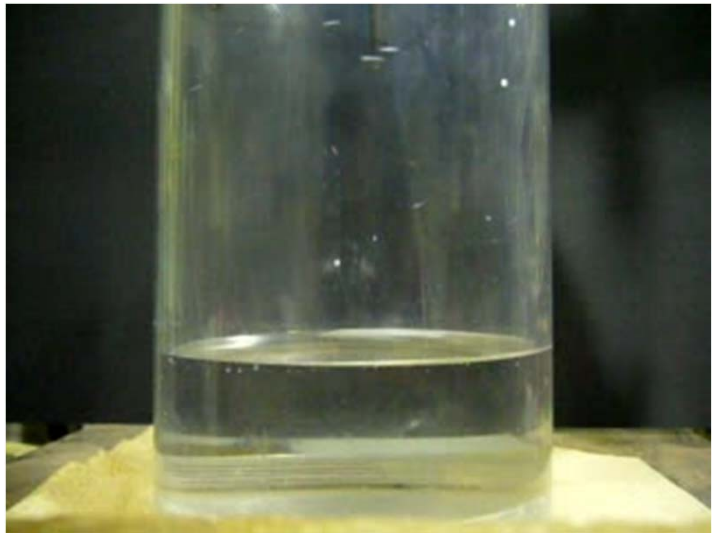

(c) $\alpha = 70^{o}$

Fig.4 Photographs in the bottom part of bust box (Q_t = 700 l/min)

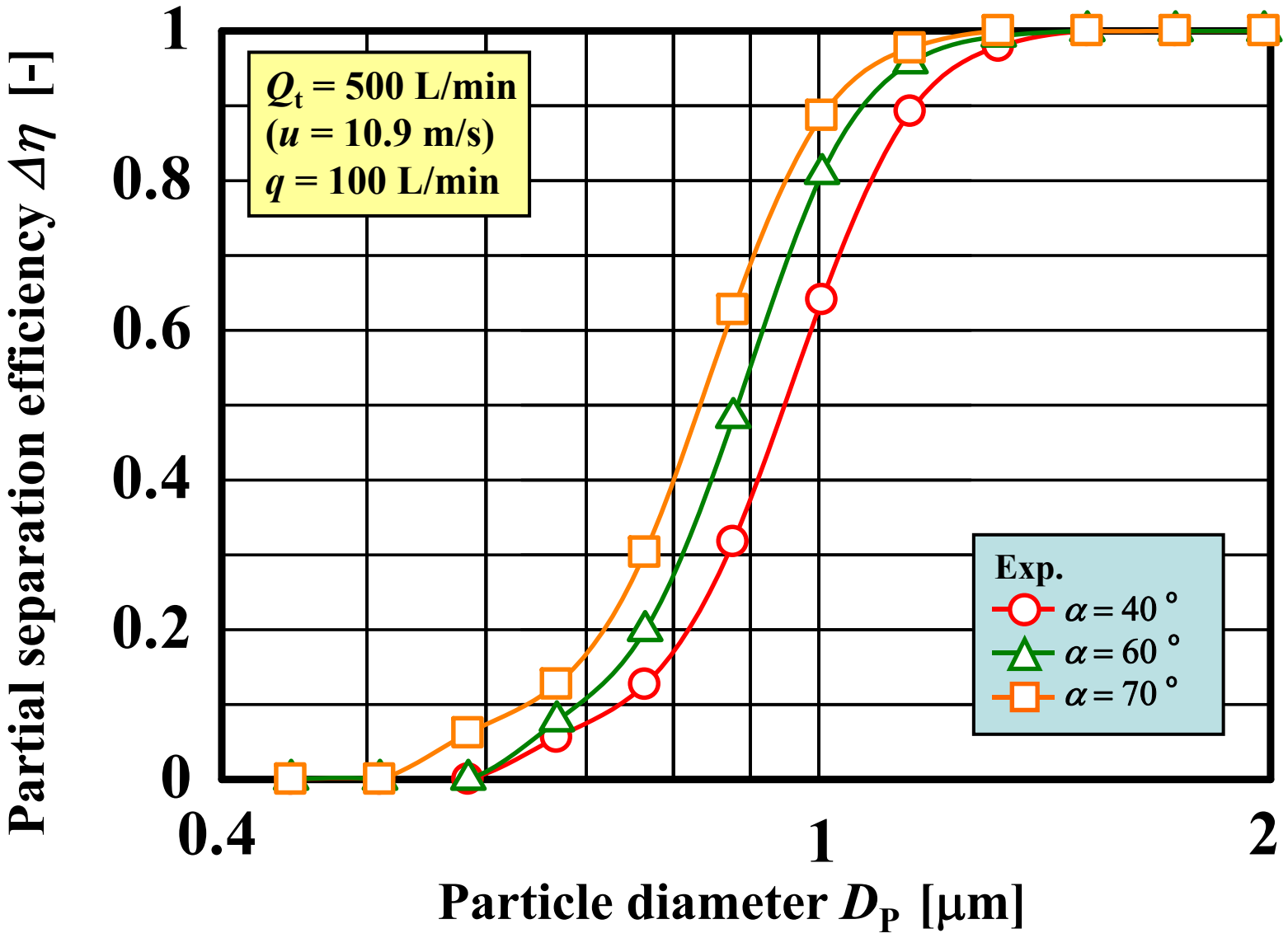

Fig.5-a Effect of apex cone angle on partial separation efficiency in the case of Q_t = 500 l/min

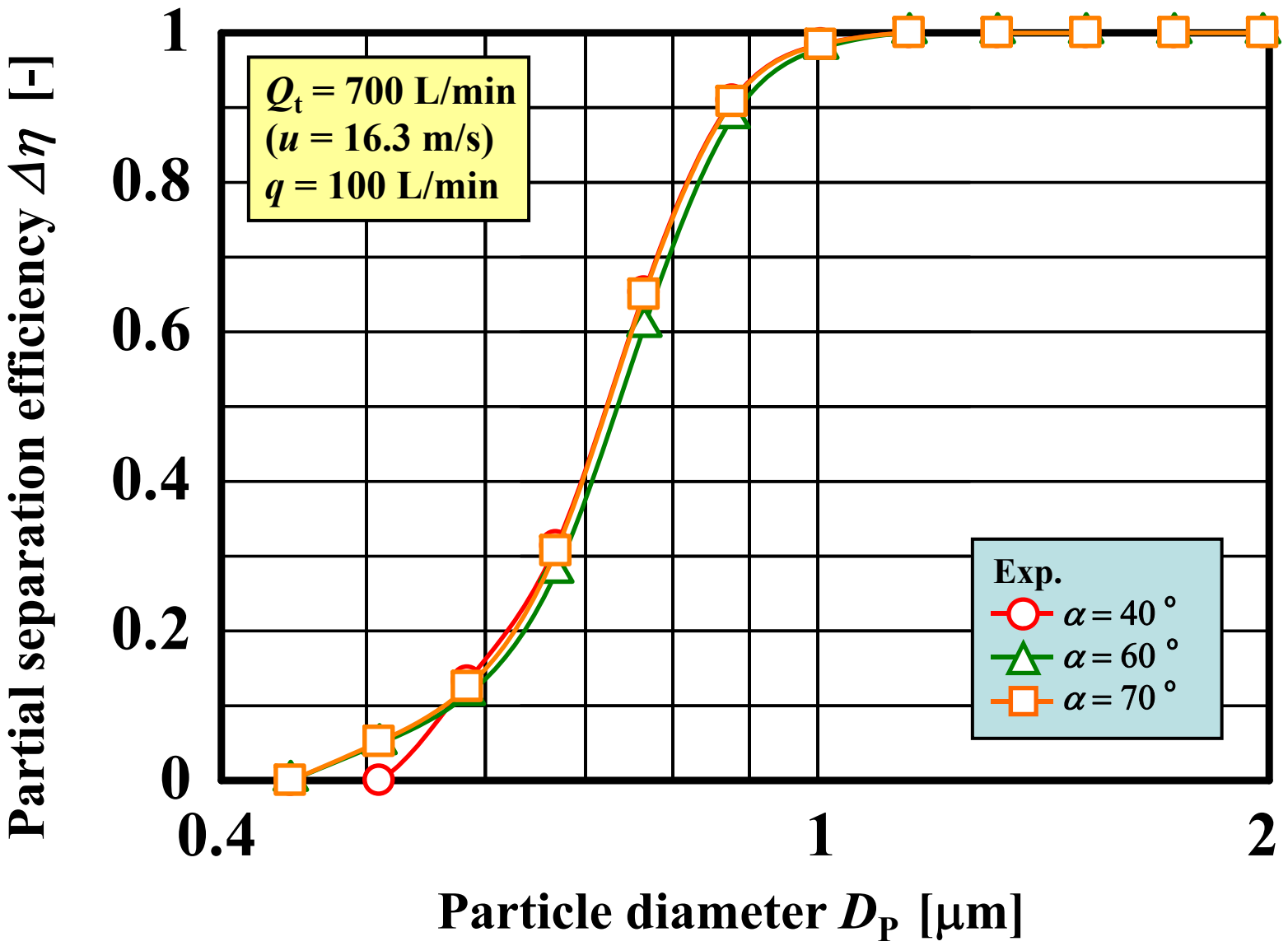

Fig.5-b Effect of apex cone angle on partial separation efficiency in the case of Q_t = 700 l/min

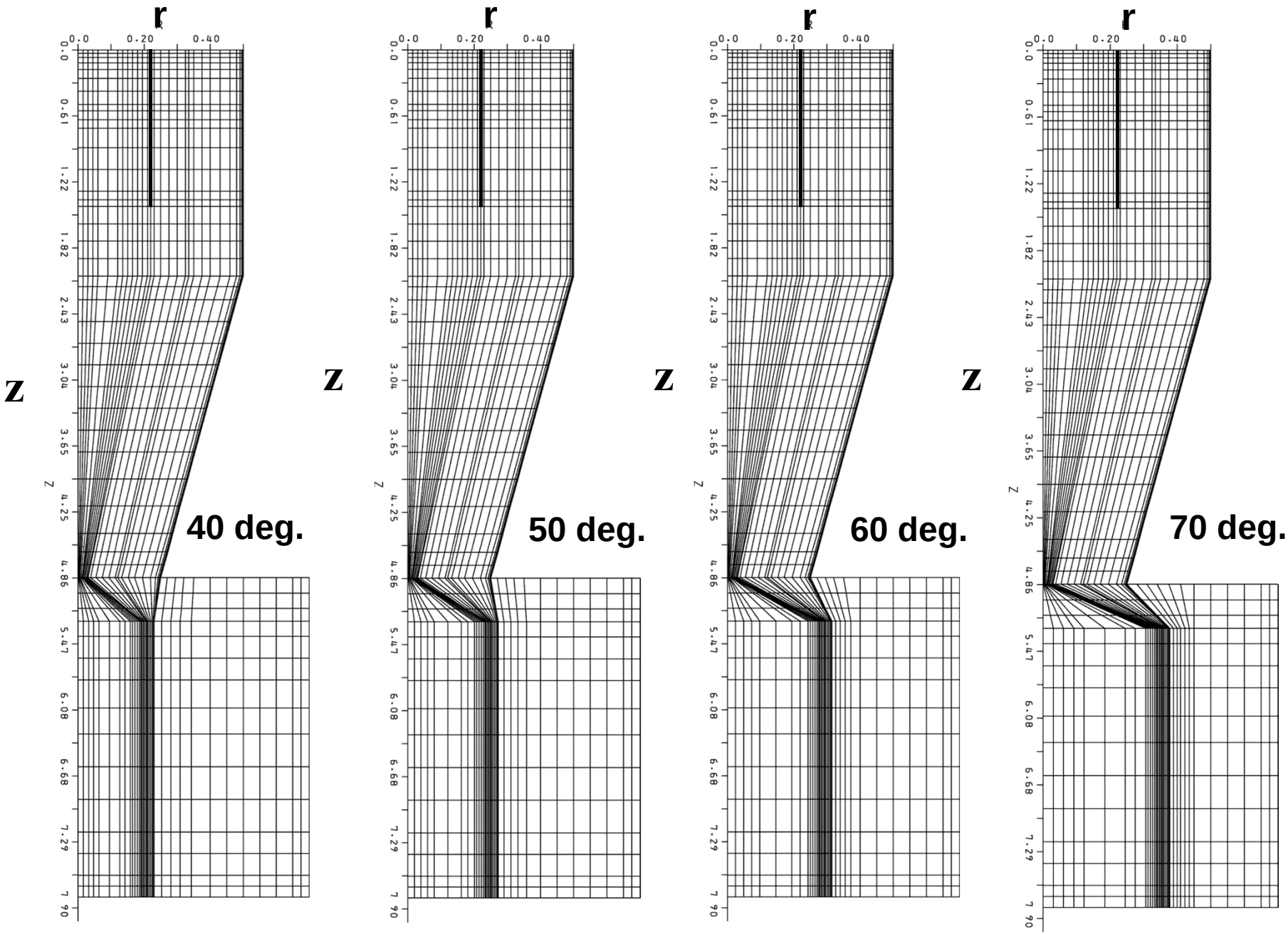

Fig.6 Grid shapes used in CFD simulation

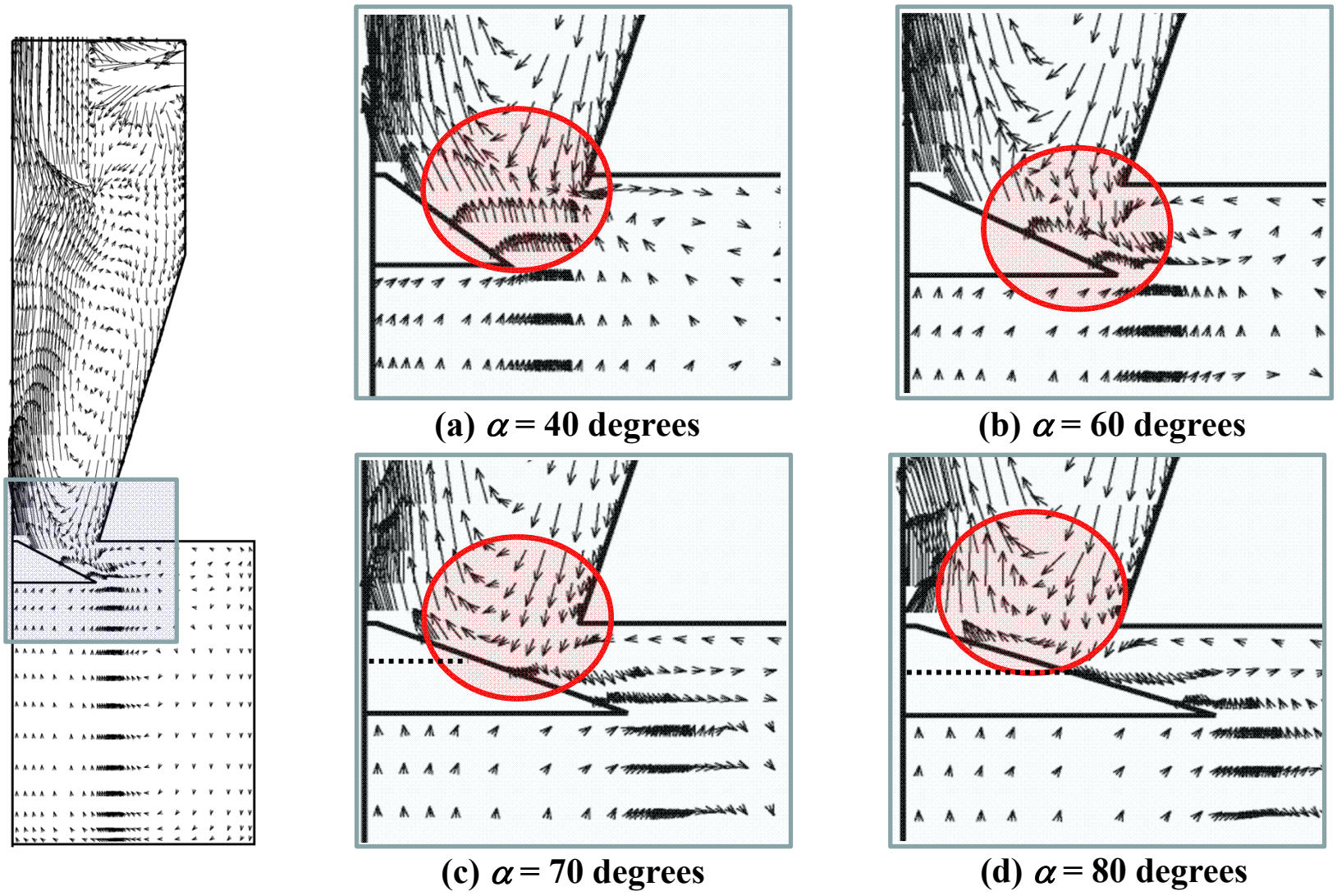

Fig.7 Fluid velocity distribution near the apex cone
(Q_t = 500 l/min, q = 100 l/min)

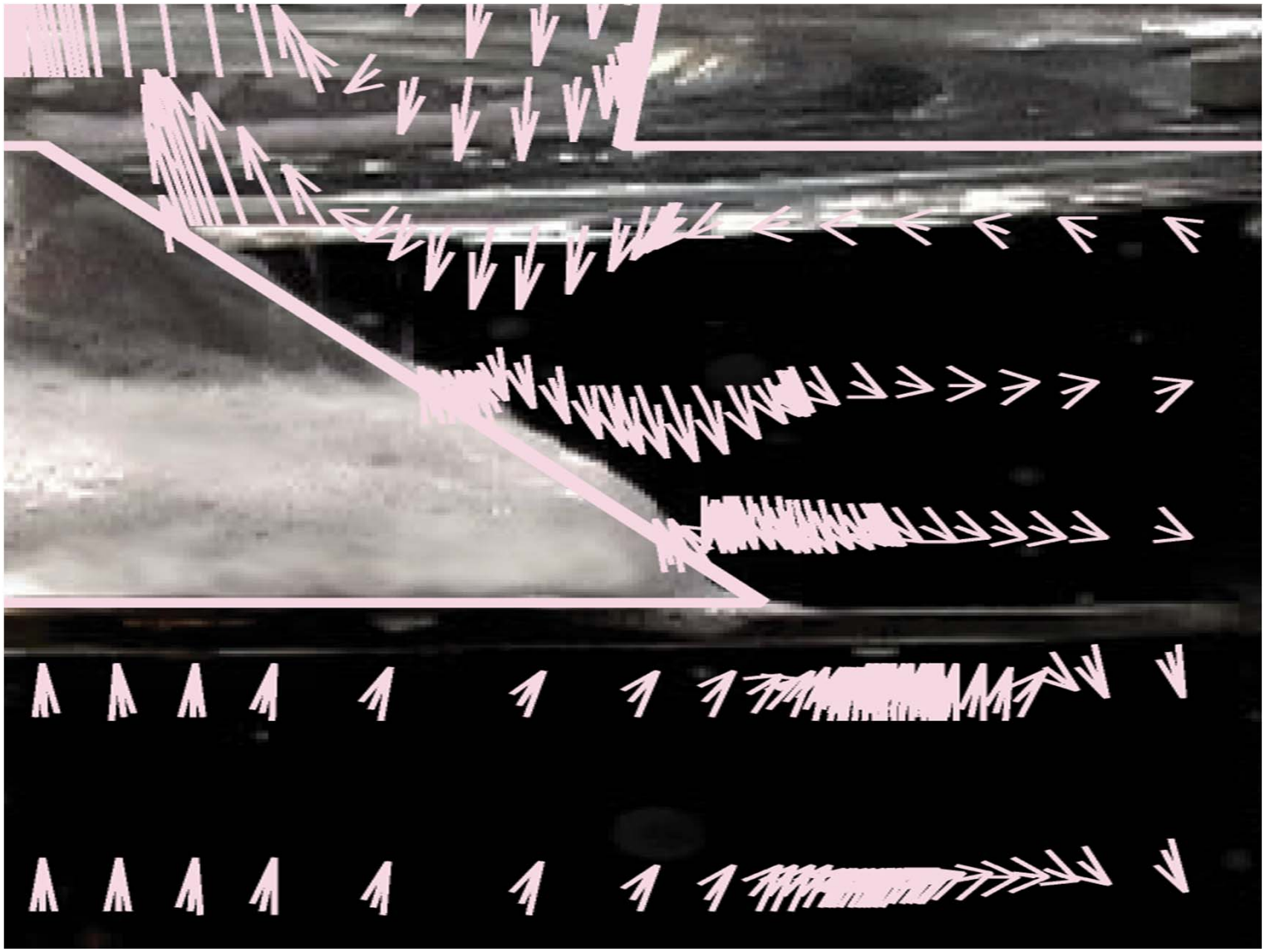

Fig.8 Fluid velocity distribution and soap foam on the 70 deg. apex cone (Q_t = 500 l/min, q = 100 l/min)

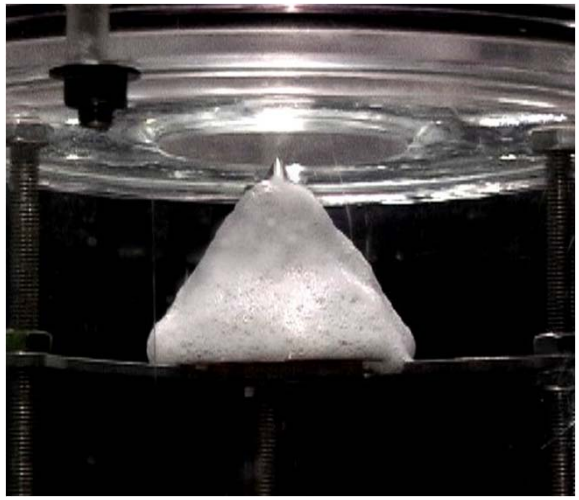

Apex cone with soap foam

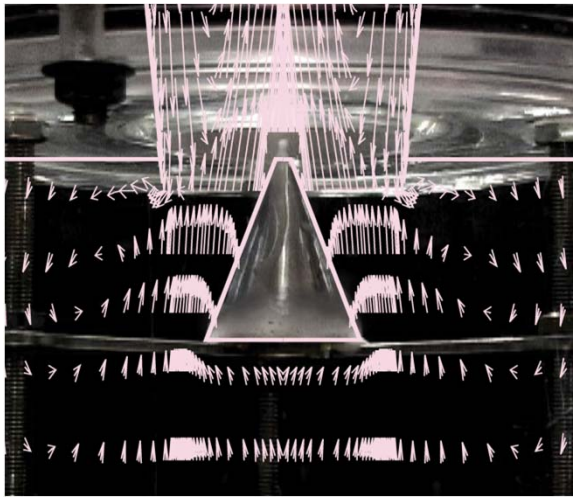

(a) $\alpha = 40$ deg.

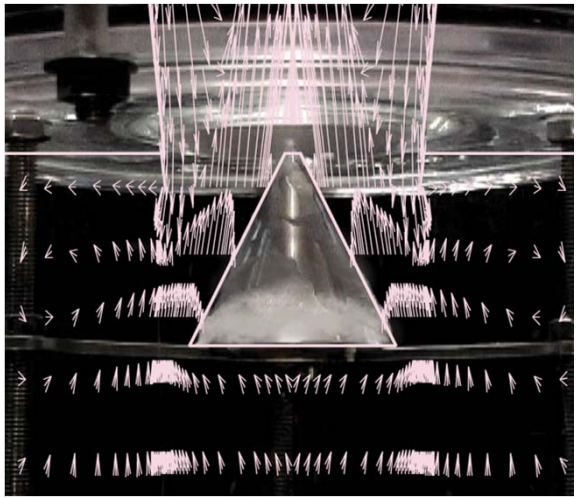

(b) $\alpha = 50$ deg.

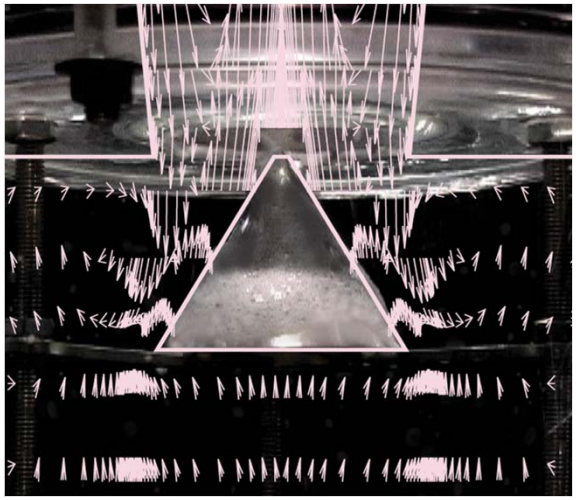

(c) $\alpha = 60$ deg.

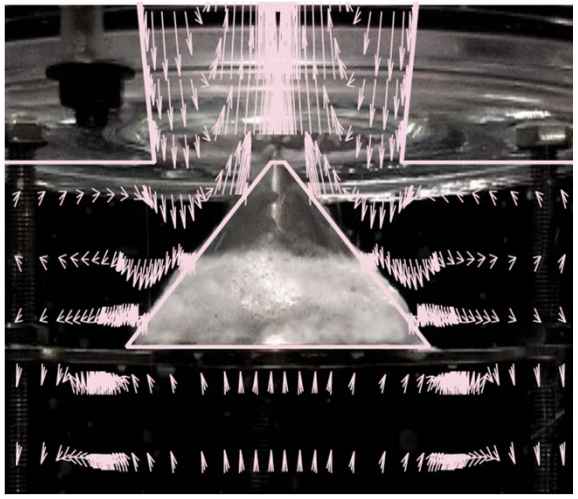

(d) $\alpha = 70$ deg.

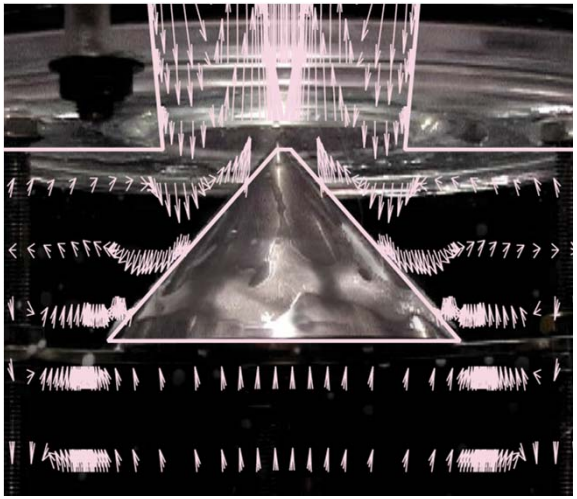

(e) $\alpha = 80$ deg.

Fig.9 Flow visualization using soap foam and calculated velocity vectors ($Q_t = 500$ l/min, $q = 100$ l/min)

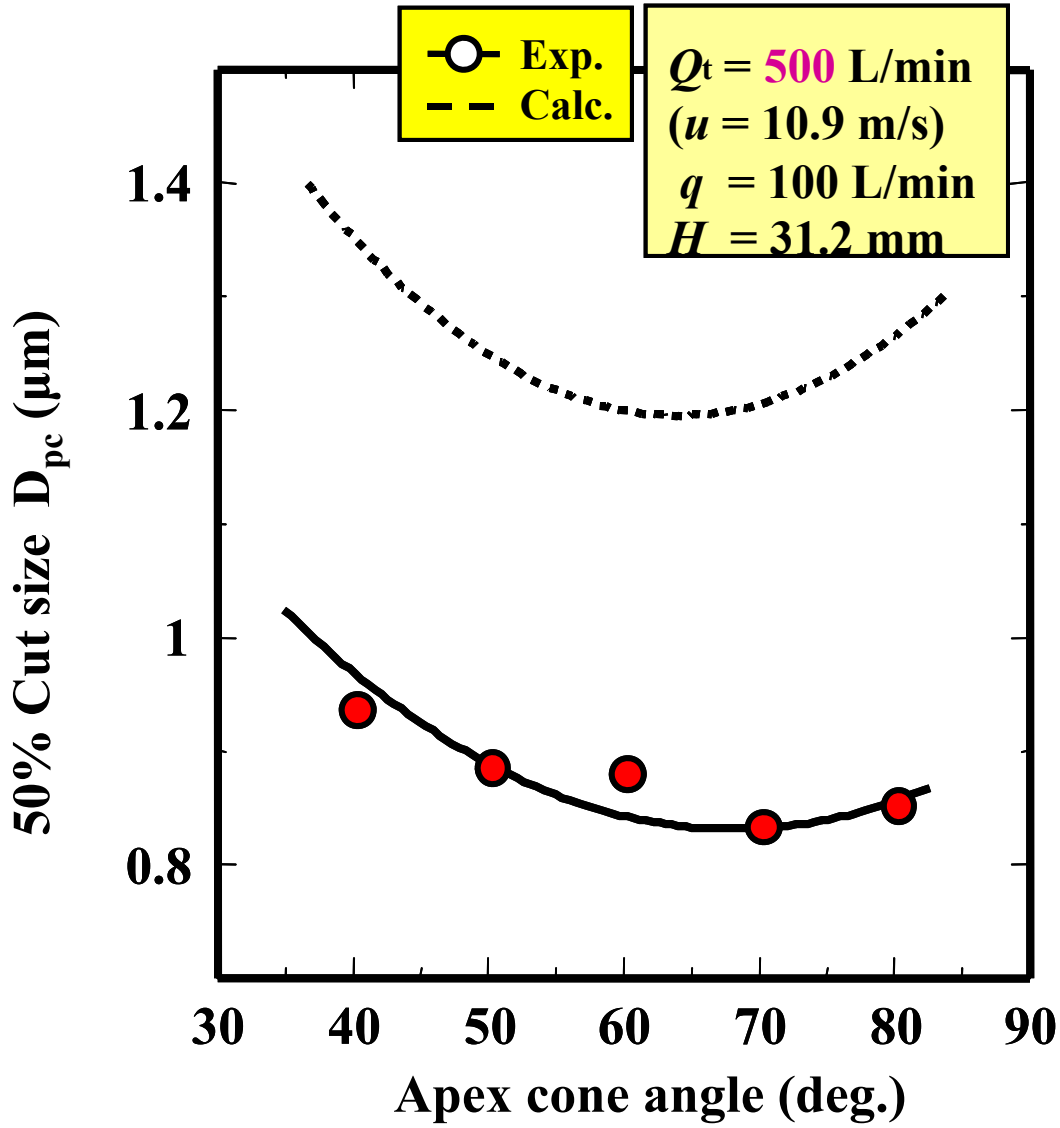

Fig.10 Effect of the apex cone angle on 50 % cut size in the case of Q_t = 500 l/min

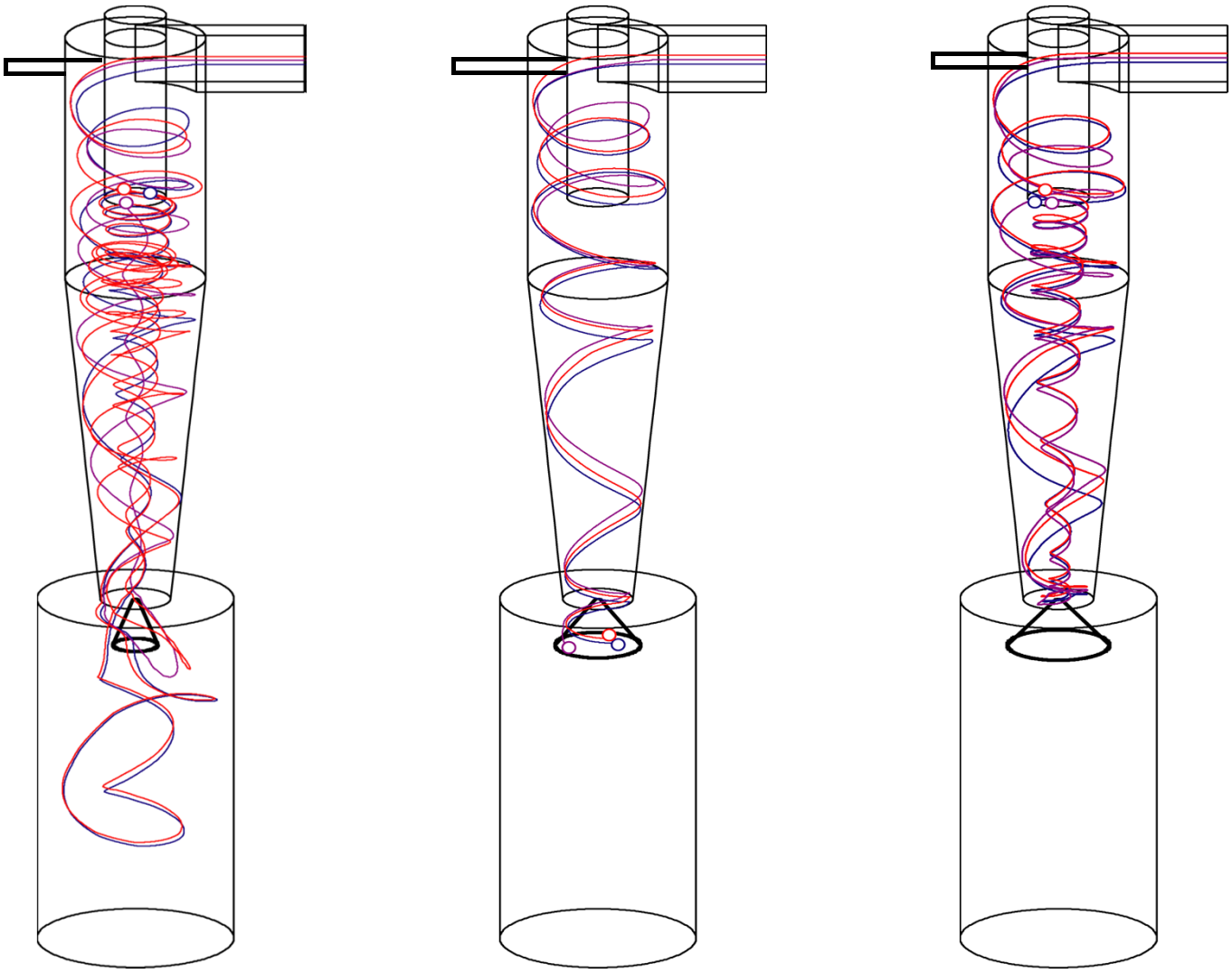

(a) α = 40 degrees (b) α = 70 degrees (c) α = 80 degrees

Fig.11 Calculated particle trajectories for three types of apex cones (D_P = 1.3 μm, Q_t = 500 l/min, q = 100 l/min)

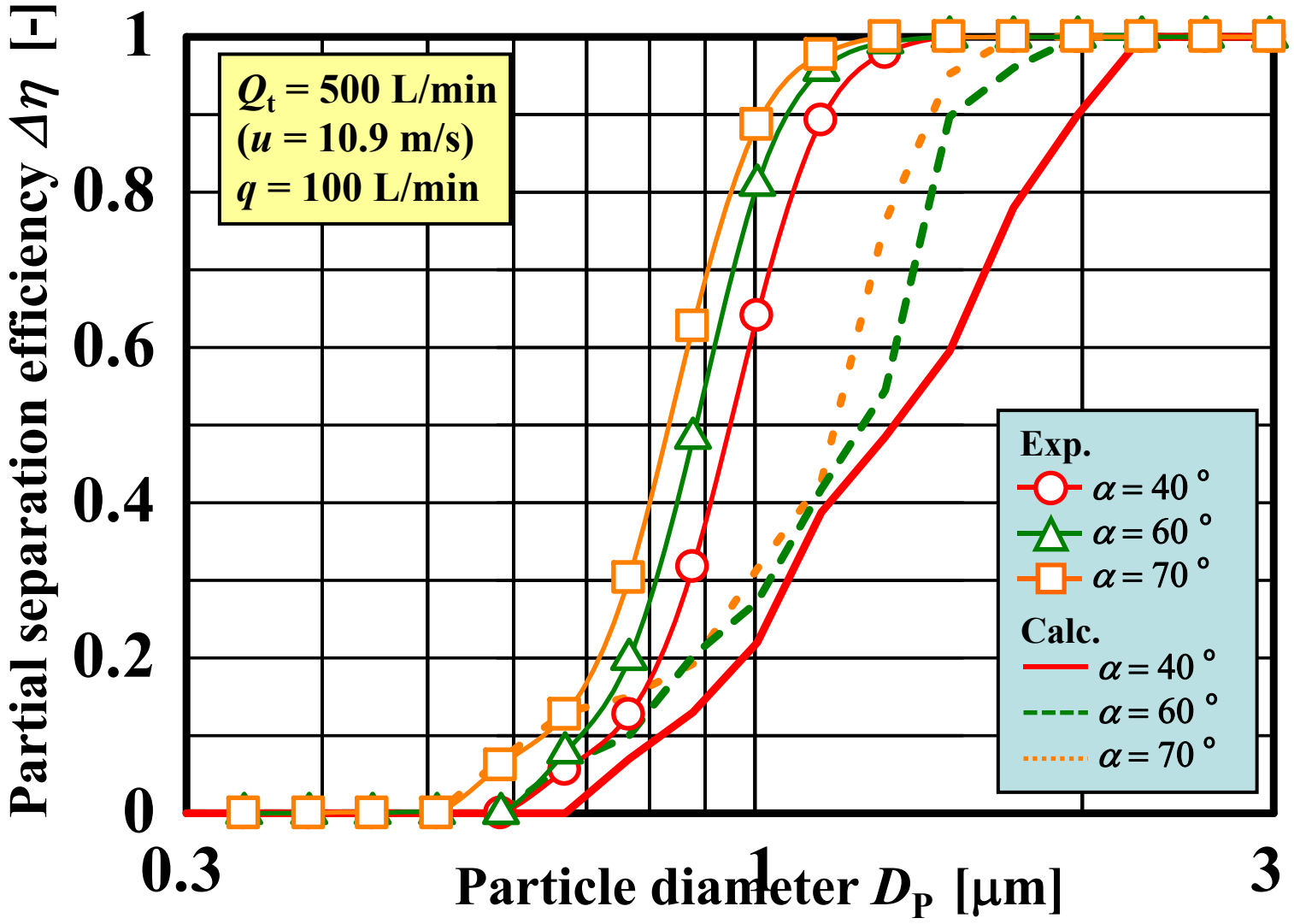

Fig.12 Effect of apex cone angle on partial separation efficiency in the case of Q_t = 500 l/min

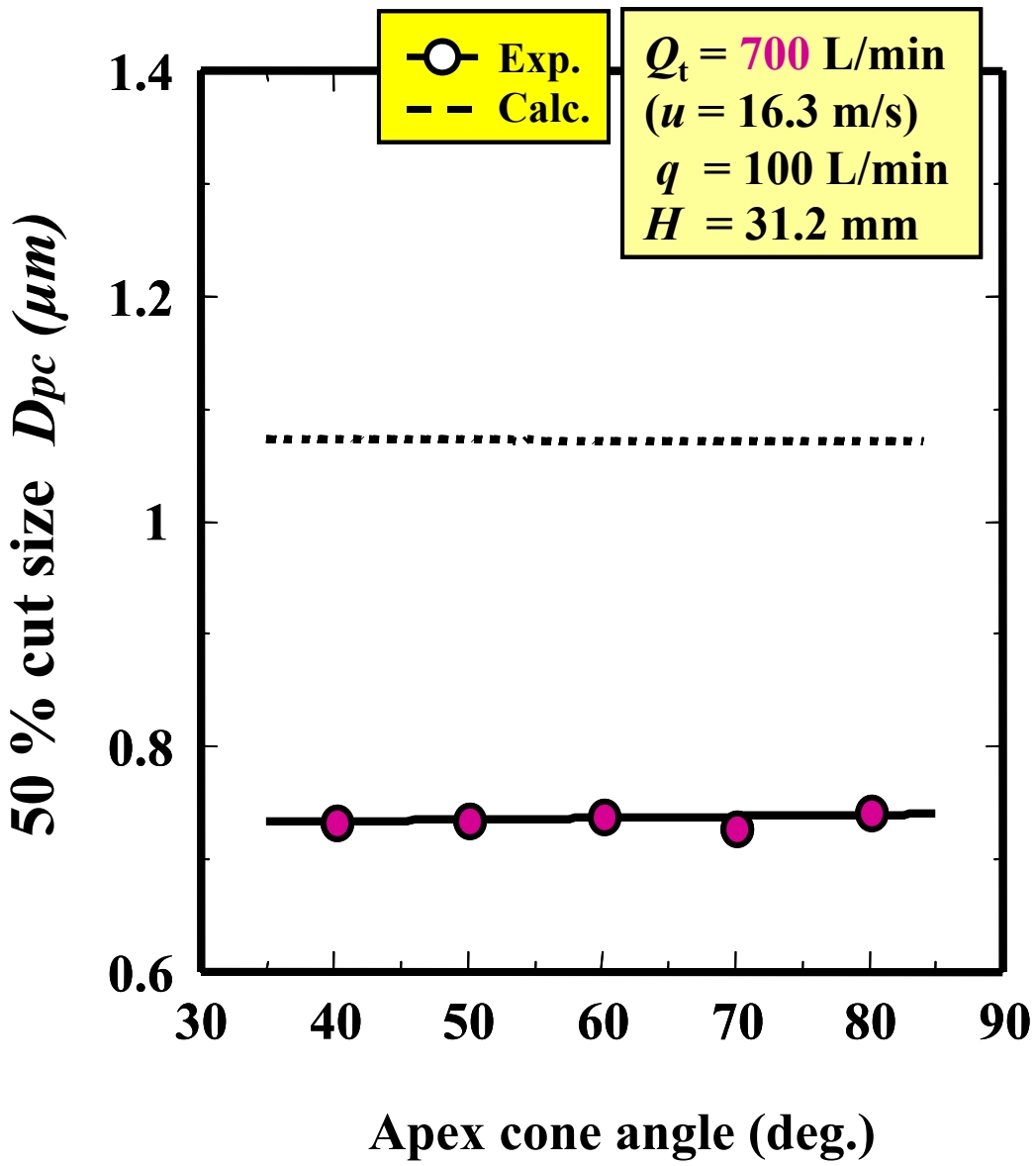

Fig.13 Effect of apex cone angle on 50 % cut size in the case of Q_t = 700 l/min

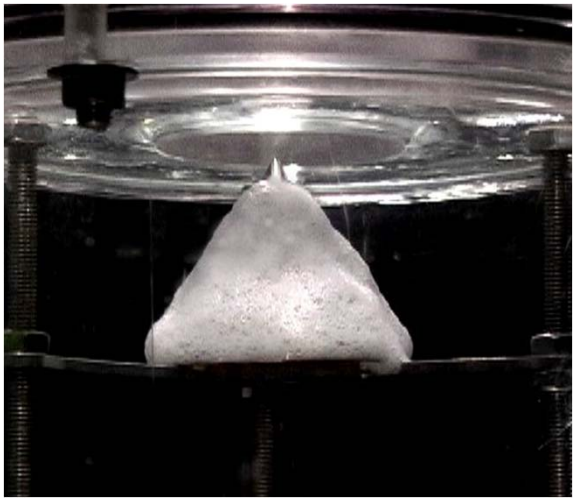

Apex cone with soap foam

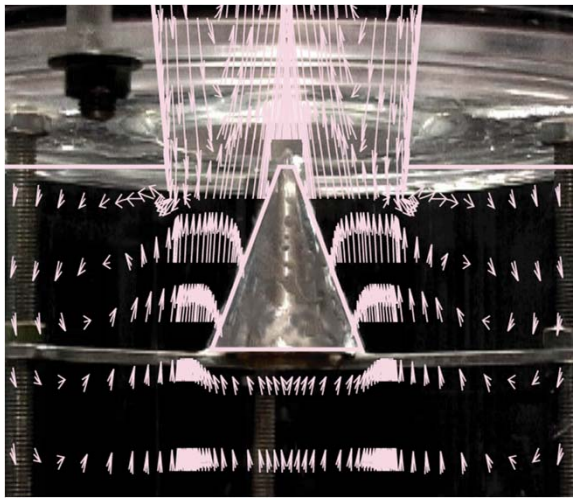

(a) α = 40 degrees

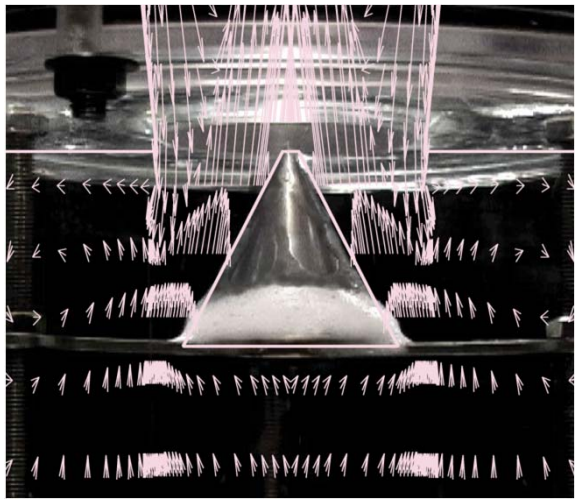

(b) α = 50 degrees

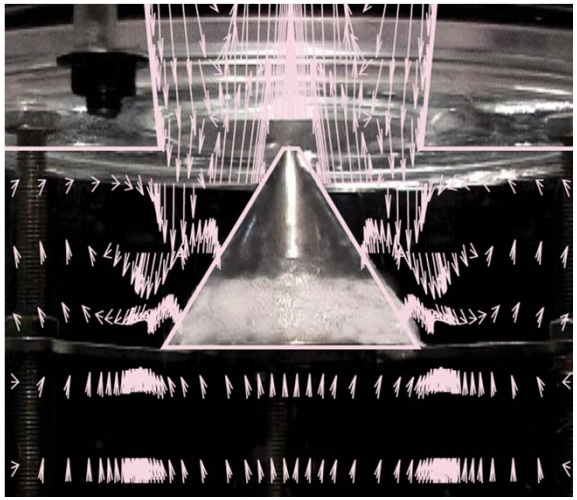

(c) α = 60 degrees

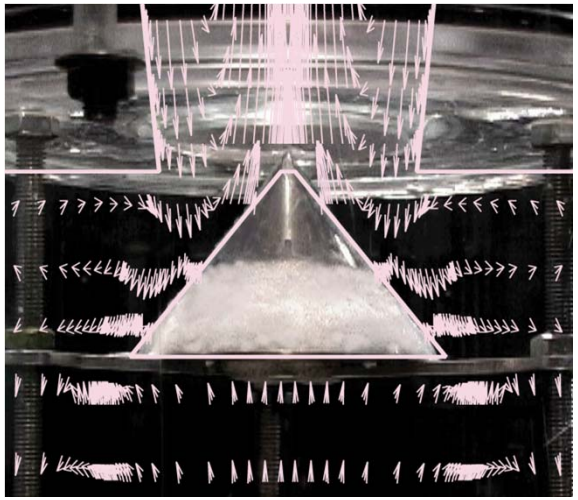

(d) α = 70 degrees

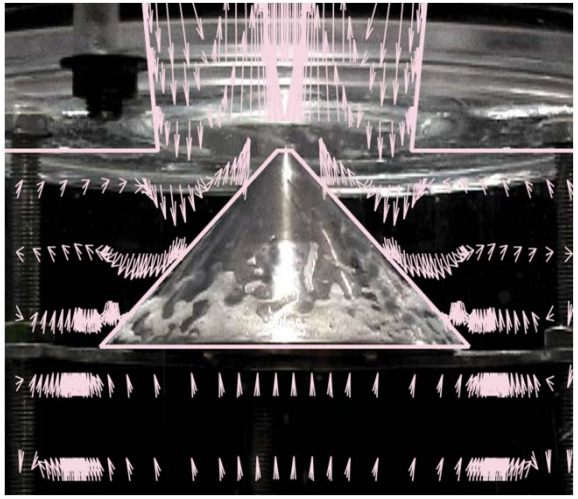

(e) α = 80 degrees

Fig.14 Flow visualization using soap foam and calculated velocity vectors (Q_t = 700 l/min, q = 100 l/min)

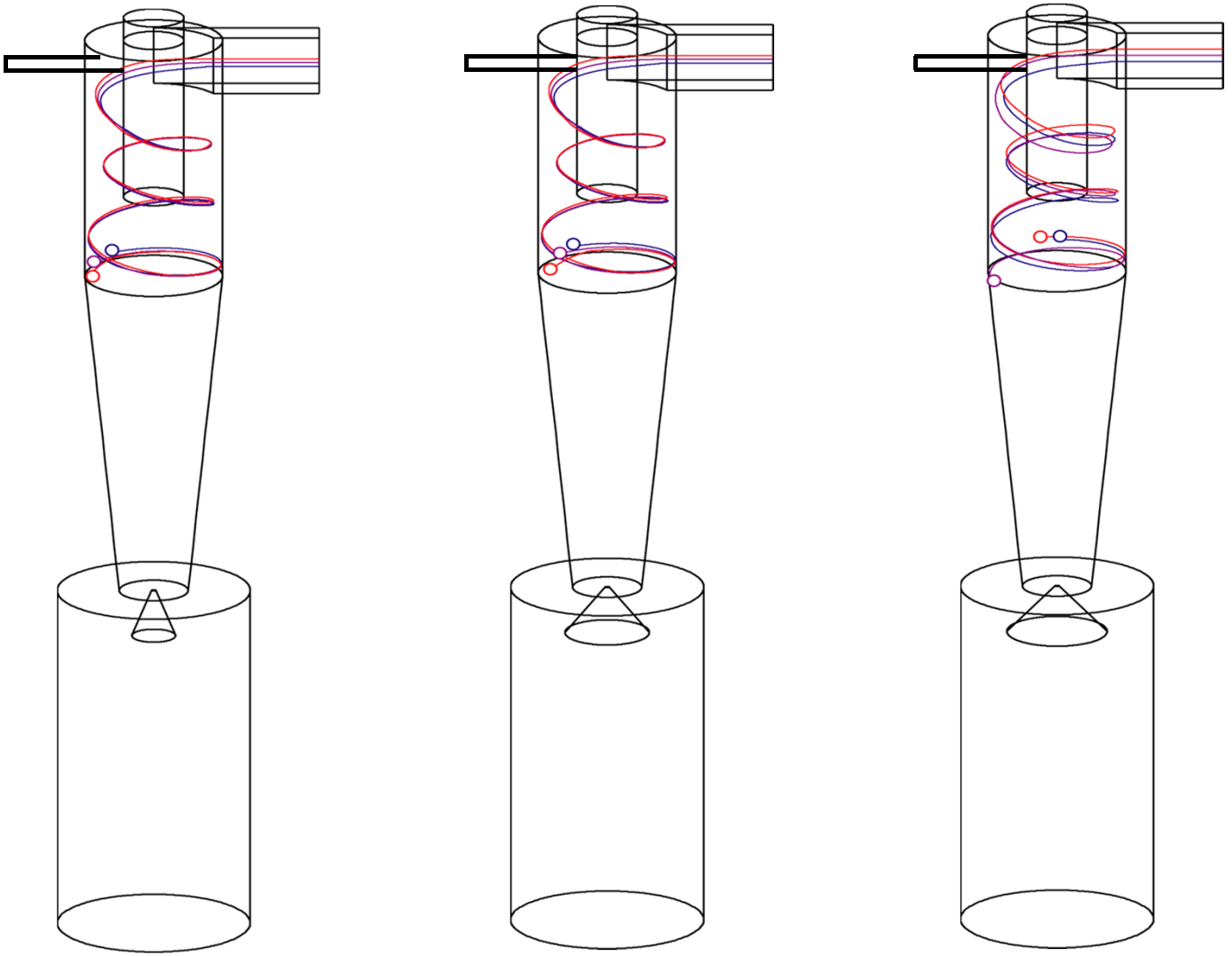

(a) α = 40 degrees (b) α = 70 degrees (c) α = 80 degrees

Fig.15-a Calculated particle trajectories for high inlet velocity condition (D_P = 1.3 μm, Q_t = 700 l/min, q = 100 l/min)

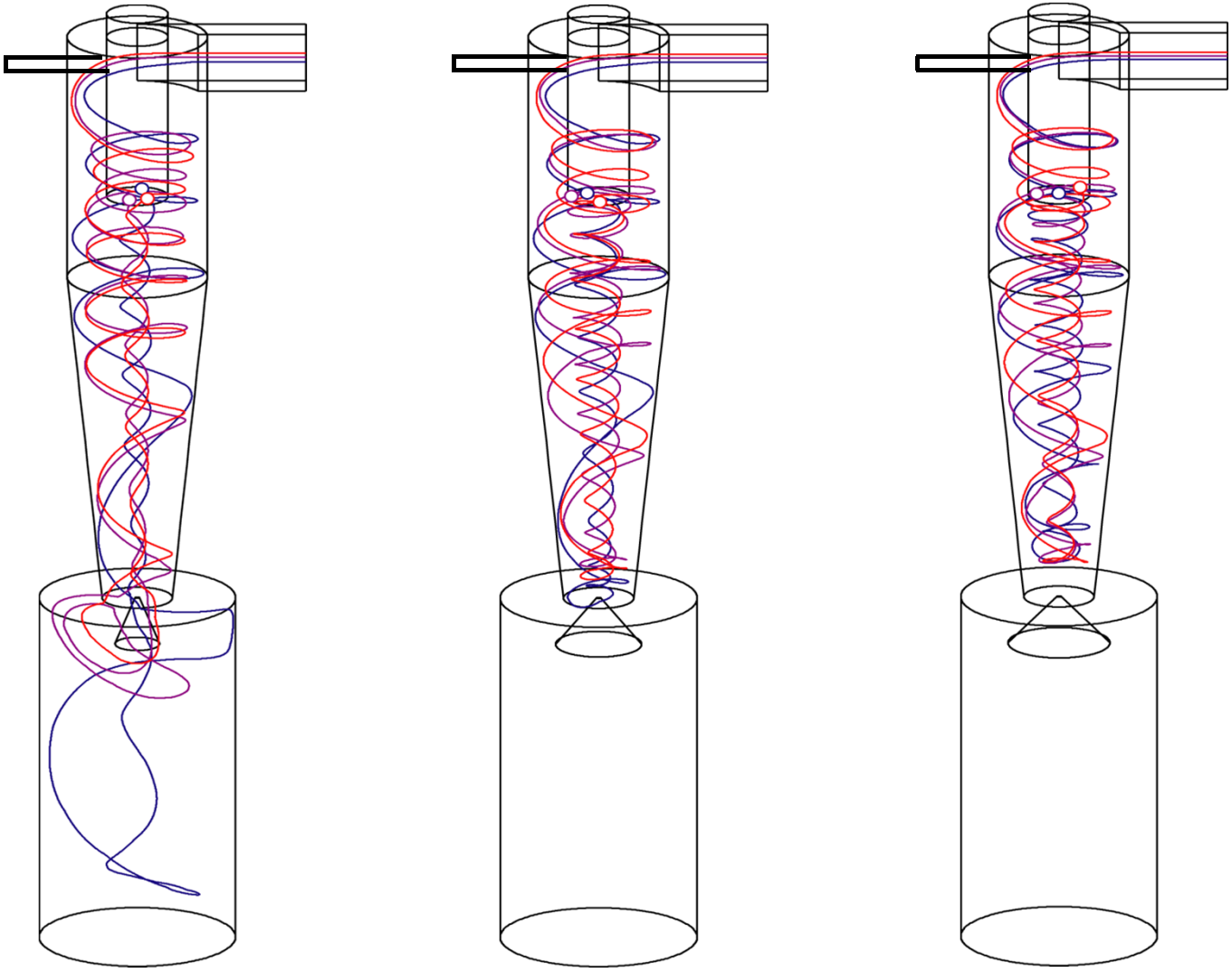

(a) α = 40 degrees (b) α = 70 degrees (c) α = 80 degrees

Fig.15-b Calculated particle trajectories for high inlet velocity condition (D_P = 1.0 μm, Q_t = 700 l/min, q = 100 l/min)

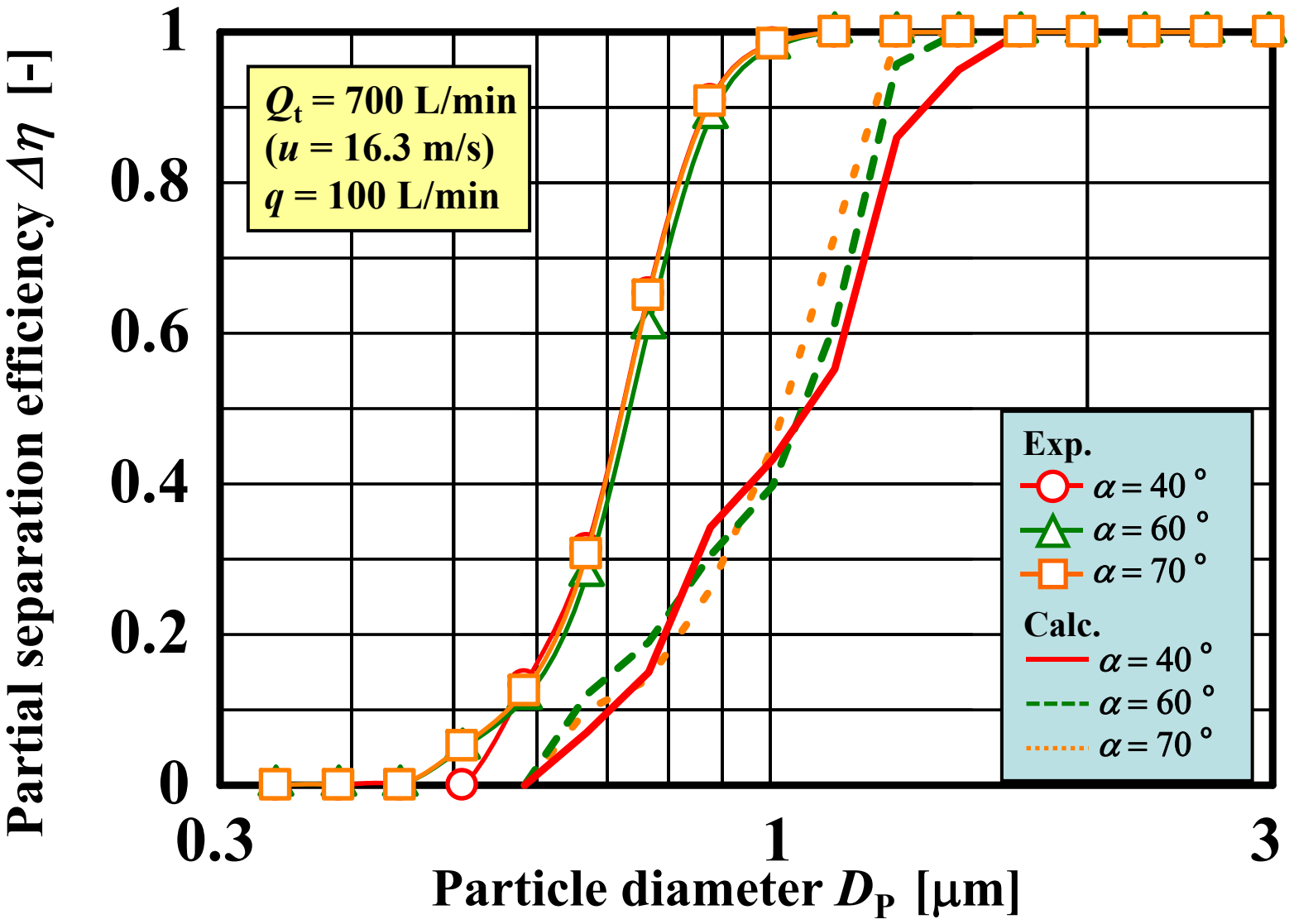

Fig.16 Effect of apex angle on partial separation efficiency in the case of Q_t = 700 l/min